Measurements and analysis of the turbulent Schmidt number in density stratified turbulence

Pablo Huq[1] and Edward J. Stewart[2]

Received 18 September 2008; revised 27 October 2008; accepted 3 November 2008; published 3 December 2008.

[1] Results are reported of measurements of the turbulent Schmidt number Sc_t in a stably stratified water tunnel experiment. Sc_t values varied with two parameters: Richardson number, Ri, and ratio of time scales, T*, of eddy turnover and eddy advection from the source of turbulence generation. For large values (T* $\sim$ 10) values of Sc_t approach those of neutral stratification ($Sc_t \approx 1$). In contrast for small values (T* $\sim$ 1) values of Sc_t increase with Ri. The variation of Sc_t with T* explains the large scatter of Sc_t values observed in atmospheric and oceanic data sets as a range of values of T* occur at any given Ri. The dependence of Sc_t values on advective processes upstream of the measurement location complicates the development of an algebraic formulation of Sc_t = f (Ri, T*) from single point dynamical balances for use in turbulence closure models. Observations of values of T* $\sim$ O(1) for strong stratification argues against the existence of a critical Richardson number at which turbulence collapses to laminar flow. **Citation:** Huq, P., and E. J. Stewart (2008), Measurements and analysis of the turbulent Schmidt number in density stratified turbulence, *Geophys. Res. Lett.*, *35*, L23604, doi:10.1029/2008GL036056.

1. Introduction

[2] Turbulent flows under conditions of stable density stratification occur ubiquitously in lakes, oceans and the atmospheres of earth and other planets. Accurate predictions of turbulent transport in a stably stratified fluid column are central to the analyses of heat transport, or buoyancy flux in general circulation models (GCMs). Such predictions are made difficult by the interplay between internal waves and turbulence which occur in a stably stratified fluid column. Complications arise in the partition when the value of the integral time scale of the turbulent flow approaches the buoyancy time scale of the fluid column because of the anisotropization of turbulence and generation of internal waves [*Sukoriansky and Galperin*, 2005; *Baumert and Peters*, 2005].

[3] Key to numerical predictions are turbulent diffusivities for scalar and momentum transport respectively defined as

$$K_\rho = \frac{-\overline{\rho w}}{\mathrm{d}\rho/\mathrm{d}z} \qquad K_m = \frac{-\overline{uw}}{\mathrm{d}U/\mathrm{d}z} \tag{1}$$

where $\overline{\rho w}$ is the buoyancy flux, $\overline{uw}$ is the Reynolds shear stress. The ratio K_m/K_ρ is termed the turbulent Schmidt number Sc_t (rather than turbulent Prandtl number) as salinity gradients in water are used for stratification in the experiments. Prescription of a functional dependence of Sc_t on $Ri = N^2/S^2$ is a turbulence closure scheme [*Kantha and Clayson*, 2000]. Here the buoyancy frequency N is defined by the gradient of density ρ as $N^2 = (-g/\rho_o)(\mathrm{d}\rho/\mathrm{d}z)$, and g is the gravitational acceleration. $S = \mathrm{d}U/\mathrm{d}z$ is the velocity shear. Analyses of field, lab and numerical (RANS, DNS and LES) data sets have led to the consensus that Sc_t increases with Ri [see *Esau and Grachev*, 2007, and references therein]. Accordingly, various forms have been suggested for Sc_t = f (Ri), for example, *Zilitinkevich et al.* [2007] gives:

$$Sc_t = Sc_o + CRi \tag{2}$$

where Sc_o is the value of the turbulent Schmidt number in the absence of density stratification ($Sc_o \approx 1$) and C = 0.3. Other forms have been suggested [e.g., *Pacanowski and Philander*, 1981; *Mellor and Yamada*, 1982]. *Cane* [1993] noted that comparison of the closure scheme of *Pacanowski and Philander* [1981] with oceanic thermocline data gave insufficient mixing at low values of Ri and too much at high values of Ri. The lack of agreement arises because Sc_t is difficult to resolve when the magnitudes of the vertical momentum flux or density gradients are small [*Esau and Grachev*, 2007]. These limitations arise for both conditions of strong stability ($Ri \to \infty$) and weak stability ($Ri \to 0$). Difficulties are compounded as there are few studies with direct measurements of the buoyancy flux $\overline{\rho w}$ and the diffusivity K_ρ is typically inferred from gradient profiles of the mean density.

[4] There is renewed interest in the precise algebraic form of this dependence following the demonstration by *Noh et al.* [2005] that numerical simulations in their GCM of the equatorial mixed layer were more realistic with the inclusion of a Sc_t dependence on stratification (i.e., Ri). Recent analyses of field data of the stable atmospheric boundary layer from polar regions [*Yague et al.*, 2001; *Esau and Grachev*, 2007] also showed an additional feature namely that $Pr_t(=Sc_t)$ values varied by more than an order magnitude at any given value of Ri. Similar spread of Sc_t values is evident in oceanic data [e.g., *Peters et al.*, 1988]. The reason for this spread or scatter is not currently known, and a unique functional dependence between Sc_t and Ri remains elusive. An emerging problem in the interpretation of data of Sc_t and Ri is the recognition of shared variables (density and velocity gradients) in plots of Sc_t versus Ri as this leads to self-correlation [*Klipp and Mahrt*, 2004; *Grachev et al.*, 2007]. The purpose of this paper is not to

[1]College of Marine and Earth Studies, University of Delaware, Newark, Delaware, USA.
[2]Visual Numerics Inc., San Ramon, California, USA.

0094-8276/08/2008GL036056

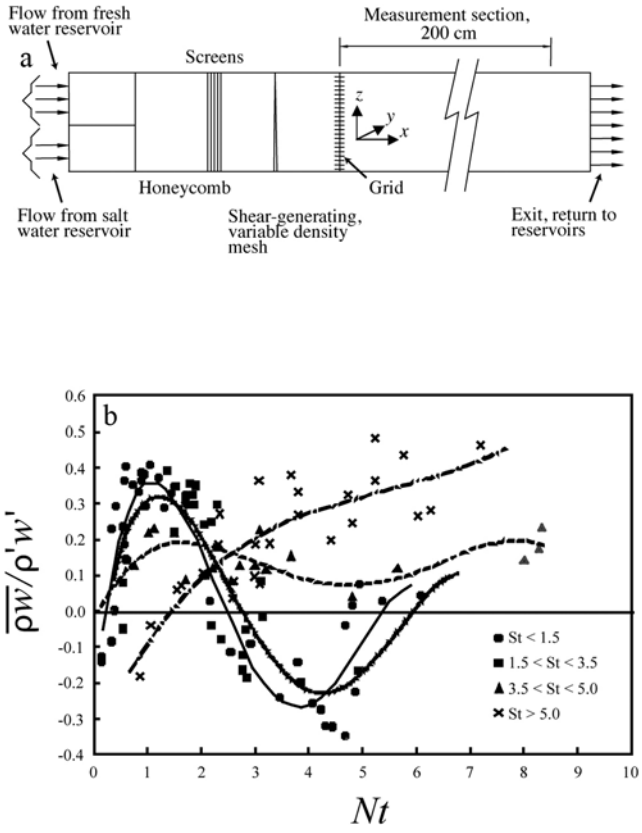

Figure 1. (a) Schematic of experimental configuration. Flow is from left to right. Free-stream noise in the incoming flow is attenuated by the honeycomb and fine screens. A sheared velocity profile is created by the variable density meshes. Turbulence is generated by a grid; the origin of the coordinate system is located at the grid. (b) Evolution of the non-dimensional buoyancy flux $\overline{\rho w}/\rho' w'$ with buoyancy time-scale ratio Nt. Data and best-fit trend lines are presented for four groups of non-dimensional shear St. The turbulence field is near shear-free for St < 1.5, and strongly sheared for St > 5. Other groups (1.5 < St < 3.5 and 3.5 < St < 5) reflect intermediate strengths of shear.

evaluate the effects of self-correlation but rather to emphasize other influences on Sc_t. In particular, we examine the role of advection on Sc_t. We undertook lab experiments to examine the form of the potential functional dependence as well as to investigate the large scatter in the values of Sc_t. The analysis described below reveals that Sc_t is not just a function of Ri but also dependent on an additional non-dimensional parameter T*, i.e.,

$$Sc_t = f(Ri, T^*) \tag{3}$$

where T* is the ratio of advective time scale to the eddy turnover time scale with explicit definitions below.

2. Experimental Method

[5] A low noise water tunnel 400cm long, 40 cm deep and 25cm wide was used for the experiments. Maximum mean velocities were 9 cm/s. Flow conditioning by a honeycomb box and fine mesh screens reduced background turbulent intensities to about 0.3% of the mean velocity. A vertical velocity gradient is created by using a variable density mesh. The stratified water column comprises a layer of fresh water above a salt water layer (see Figure 1a). Turbulence is generated using a bi-plane grid of square bars of width d = 0.64 cm, arranged in a mesh with spacing M = 3.2 cm, such that M/d = 5. The maximum mesh Reynolds number $Re_M = UM/\nu$ is approximately 2700. The density and velocity gradients vary in the vertical direction (both are approximately linear in the center of the water tunnel). Integral length scales (typically M/3) were much smaller than the vertical extent of the linear gradient region (typically 3M). This allows scaling by the density gradient, N, and velocity gradient, S. Values of N and S were varied so that there is a large domain space of *Nt* and *St* values (the dimensionless strain rates used to gauge the importance of stratification and shear). The above dimensionless quantities are constructed using $t = x/U$, yielding $Nt = Nx/U$ and $St = Sx/U$. The set-up allows for values of *Nt* and *St* up to about 9.

[6] The density field was measured using an aspirating conductivity probe with a spatial resolution of 0.04cm and frequency response of 70 Hz. The velocity field was measured using quartz-coated, two-component hot film probes (TSI type 1241-20w), powered by an anemometer at 2% overheat ratio. Direct measurements of buoyancy flux ($\overline{\rho w}$) were obtained by simultaneously operating the conductivity and hot-film probes, located 0.1cm apart. The errors in rms fluctuations and correlations were estimated to be 5% and 10%, respectively. We present results in non-dimensional form. Dimensional values (including evolution of velocity variances and spectra) and further details of the apparatus and measurement techniques are given by *Stewart and Huq* [2006].

3. Results

[7] The measured evolution of the normalized buoyancy flux $\overline{\rho w}/\rho' w'$ is shown in Figure 1b. Data are grouped into four categories of increasing strengths of shear ranging from near shear-free turbulence (St < 1.5) to strongly sheared turbulence (St > 5). The normalized buoyancy flux attains maximum values of 0.4 for near shear-free turbulence at Nt $\sim$ 1 and attenuates to small even negative values (counter gradient flux) for larger values of Nt. The evolution of buoyancy flux differs with increasing values of shear. Generally, away from the grid, values of $\overline{\rho w}$ are positive for sheared turbulence. These trends for the evolution of buoyancy flux for both weak shear and strong shear are in excellent accord with previous studies of shear-free turbulence [*Itsweire et al.*, 1986; *Huq and Britter*, 1995] and sheared turbulence [*Rohr et al.*, 1988; *Piccirillo and Van Atta*, 1997]. The buoyancy flux measurements are used to calculate diffusivities K_ρ as in equation (1). Measurements of the turbulent Schmidt number Sc_t are plotted as a function of the Richardson number Ri in Figure 2a. Values of Sc_t range from approximately 1 at Ri $\sim$ 0.1 to about 10 at Ri $\sim$ 10. Although scattered at high Richardson numbers, the data show two trends. First, values of Sc_t generally increase with Ri; second, for small values of Ri less than 0.1, values of Sc_t asymptotically approach the limit of $Sc_t \approx 1$ for the case of neutral stratification. Again note that the

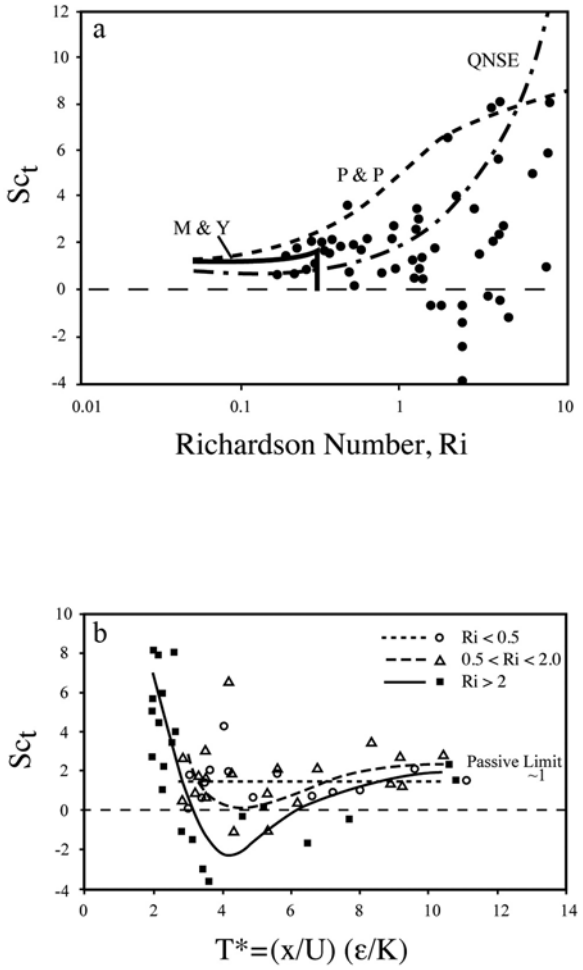

Figure 2. (a) Dependence of turbulent Schmidt number Sc_t on Richardson number Ri. Note that values of Sc_t and the range or spread of data increases with Ri. Also shown are the predictions of the turbulence closure models of *Pacanowski and Philander* [1981], *Mellor and Yamada* [1982], and the QSNE theory of *Sukoriansky et al.* [2005]. (b) Evolution of Sc_t with non-dimensional time T*, the ratio of advective to eddy decay time scales. Data and best-fit trend lines are shown for weak, intermediate and strong stratification (Ri < 0.5, 0.5 < Ri < 2, Ri > 2 respectively). For large values T* $\sim$ 10 values of Sc_t approach the value ($\approx$1) of passive or neutral stratification and are independent of Ri.

data are scattered and that the spread increases with Ri. This is similar to other studies. Also shown on Figure 2a are the predictions of the turbulent closure schemes of *Mellor and Yamada* [1982] and *Pacanowski and Philander* [1981] as well as the quasi-normal scale elimination approach (QSNE) of *Sukoriansky et al.* [2005]. The trends of these closure schemes also show that Sc_t increases with Ri. Note that the *Mellor and Yamada* [1982] scheme reverts to background values for Ri > 0.3, and that the *Pacanowski and Philander* [1981] scheme forms an approximate upper bound to the data.

[8] Analysis of timescales of the flow (see Figure 1a) provides insight into the above trends. Specifically, consideration of the relative magnitudes of the eddy turnover time, the time scale of energy transfer from large to small eddies, $T_E = K/\varepsilon$ [*Tennekes and Lumley*, 1982] and the advective time scale $T_A = x/U$ (the travel time from the locus of turbulence generation) provides dynamical insights for the spread of the data. Here ε is the dissipation rate of turbulent kinetic energy K. The ratio of timescales T_E and T_A yields a non-dimensional eddy decay timescale:

$$T^* = T_A/T_E = \frac{x}{U}\frac{\varepsilon}{K} \tag{4}$$

Eddies, generated previously at an upstream location, advect past a measurement station: the speed of advection is important. Qualitatively the effect of a rapidly overturning eddy that is being advected rapidly is similar to that of a slowly overturning eddy that is being advected slowly. For both cases T* $\sim$ O(1). This reflects an interplay between advection and overturning. For T* $\sim$ O(1) overturning effects dominate: buoyancy effects influence overturning in this regime yielding a strong dependence of Sc_t on Ri. For T* $\gg$ 1 the range of variations of Sc_t values are small. At a measurement location eddies may be advected past that are at different stages in their evolution. T* is a measure of the overturning of eddies. At any location variations of Sc_t values arise over a period of time due to the range of values of T*.

[9] The dependence of measured Sc_t data on the non-dimensional decay time scale T* presented in Figure 2b can be used to ascertain various aspects of the dynamics of turbulent density stratified flow. The data appears to be scattered in Figure 2b. To aid the reader the data has been grouped into 3 groups according to stratification: weakly stratified turbulence, Ri < 0.5, whose dynamics are akin to neutrally stratified (or passive) turbulence; strongly stratified turbulence Ri > 2; and an intermediate in-between state where 0.5 < Ri < 2. Best-fit trend lines have been drawn through each group. For weak stratification, Sc_t values are independent of T*, and the value of the trend line is close to the value of the passive limit ($Sc_t \sim 1$). Values of Sc_t vary with T* for intermediate and strong stratification. Figure 2b also shows that the trend lines for all three strengths of stratification converge to the value $Sc_t \sim 1$ for large values of T* $\sim$ 10: this demonstrates that Sc_t values are independent of Ri for large values of T*. In contrast for small values of T* $\sim$ 1 there is a large range of values of Sc_t.

[10] The complications of stable stratification are evident in the departures of the trend lines from the passive limit for both groups, 0.5 < Ri < 2 and Ri > 2, in Figure 2b. Broadly, for intermediate and strongly stratified conditions, Sc_t values vary non-monotonically with T*. For example, the trend line for intermediately stratified data show that Sc_t values decrease with T* up to T* $\sim$ 4; values subsequently increase and approach values of the passive limit ($\sim$1) for T* > 4. The direct consequence of stratification is the attenuation of the buoyancy flux, $\overline{\rho w}$, and turbulent diffusivity, K_ρ, so that Sc_t values increase [*Turner*, 1973]. This behavior is well reproduced by numerical models [e.g., *Sukoriansky and Galperin*, 2005; *Jimenez and Cuxart*, 2005]. The indirect effect of stratification arising from the consequences of decay and advection of eddies, however, has not been fully appreciated. To reiterate, the experimental

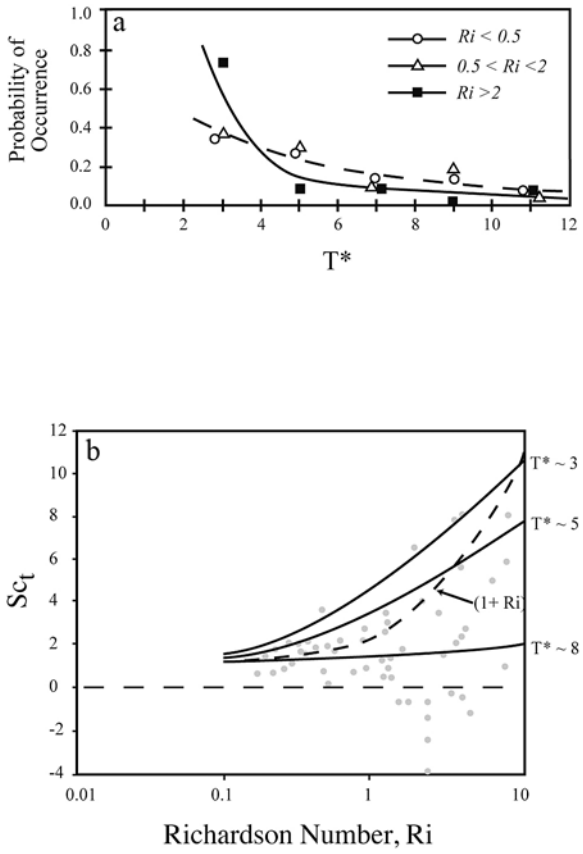

Figure 3. (a) Probability of occurrence of T*. For all three cases of weak, intermediate and strong stratification values of T* $\sim$ 1 are more likely than T* $\sim$ 10. (b) Dependence of Sc_t on Ri and T*. Solid lines are drawn through the data for T* $\sim$ 3, 5, 8. Sc_t increases with Ri for small values T* $\sim$ 3. Sc_t values are similar to those for neutral stratification ($\sim$ 1) for large values of T* $\sim$ 8. The dashed line $Sc_t = (1 + Ri)$ indicates an approximate best-fit through the data.

data are not scattered; rather, Sc_t values vary due to a distribution in values of T*. Advection complicates the analysis as mixing processes at a location in the flow are dependent on the flow dynamics upstream. Values of Sc_t for strongly stratified data (Ri > 2) become negative over the range 3 < T* < 6 due to the relatively large (negative) contribution from counter-gradient transport to buoyancy flux (see Figure 1b) as the flow attempts to re-stratify after the perturbation of passage through the turbulence grid. It is evident that turbulent stably stratified flow comprises a complex mix of down-gradient and counter-gradient buoyancy flux in addition to internal waves. Counter gradient transport attenuates for larger values T* $\sim$ 10, allowing Sc_t values to become positive again.

[11] The probability of occurrence of T* is shown in Figure 3a. It is evident that small values of T* (<3) are most common and that larger values of T* are more rare for all three strengths of stratification. The overall trends, taking into account longevity and advection of eddies as well as stratification, are shown in Figure 3b. Here Sc_t values are plotted as a function of Ri and T* and trend lines are drawn through the data for T* $\sim$ 3, 5 and 8. The line for T* $\sim$ 3 forms an upper bound to the envelope of measured Sc_t values while a line for T* $\sim$ 8 forms a lower bound for Sc_t values. The dashed curve $Sc_t = (1 + Ri)$ is a reasonable best fit through the middle of the data.

[12] Critical values of R_i have been postulated for which turbulence is extinguished and buoyancy flux ceases [*Miles*, 1961; *Howard*, 1961; *Abarbanel et al.*, 1984]. This results in a discontinuous evolution of Sc_t with Ri. The concept of a critical Richardson number has been recently questioned by *Galperin et al.* [2007] and *Zilitinkevich et al.* [2007]. The data of Figure 2a shows no discontinuity at Ri = 0.25 or 1. Figure 3a shows that the effect of strong stratification is to decrease the probability of occurrence of overturning eddies with large values of T*; however, there is no extinction of turbulence as overturning eddies with small values of T* $\sim$ O(1) still occur. This argues against the existence of a critical Richardson number.

4. Conclusions

[13] Experiments were performed on stably stratified turbulence in a water tunnel. Turbulent velocity, density fields and buoyancy flux were measured to determine the turbulent Schmidt number Sc_t. Sc_t values were dependent on two parameters, Ri and T* representing the strength of stratification, and the non-dimensional eddy turnover timescale. The dependence of Sc_t on T* had not been identified previously. The scatter observed in Sc_t data sets measured in the atmosphere and ocean as well as in the present lab data arises from the range or distribution in T* values at any given value of Ri. For large values T* $\sim$ 10 the value of Sc_t is independent of Ri and equal to the value ($\approx$1) for neutral stratification. Values of Sc_t increase with Ri for small values T* $\sim$ O(1) where a best fit to the data is $Sc_t = (1 + Ri)$. The prospect for a unique prescription of Sc_t based on single point dynamical balances in density stratified turbulence is complicated further by the fact that Sc_t is dependent on advection (i.e., what happens upstream of the measurement location). The observation of values of T* $\sim$ O(1) for strong stratification suggests that there is no critical value of Ri at which turbulence collapses to laminar flow.

References

Abarbanel, H., D. Holm, J. Marsden, and T. Raitu (1984), Richardson number criterion for the non-linear stability of three-dimensional stratified flow, *Phys. Rev. Lett.*, *52*, 2352–2355.

Baumert, H. Z., and H. Peters (2005), A novel two-equation turbulence closure for high Reynolds numbers. Part A: Homogeneous, non-rotating stratified shear layers, in *Marine Turbulence: Theories, Observations and Models*, edited by H. Baumert, J. Simpson, and J. Sündermann, chap. 3, pp. 14–30, Cambridge Univ. Press, Cambridge, U. K.

Cane, M. (1993), Near-surface mixing and the ocean's role in climate, in *Large Eddy Simulation of Complex Engineering and Geophysical Flows*, edited by B. Galperin and S. Orszag, pp. 489–509, Cambridge Univ. Press, Cambridge, U. K.

Esau, I. N., and A. A. Grachev (2007), Turbulent Prandtl number in stably stratified atmospheric boundary layer: Intercomparison between LES and SHEBA data, *e-WindEng*, *2007* (006), 1–17.

Galperin, B., S. Sukoriansky, and P. S. Anderson (2007), On the critical Richardson number in stably stratified turbulence, *Atmos. Sci. Lett.*, *8*, 65–69, doi:10.1002/asl.153.

Grachev, A. A., E. L. Andreas, C. W. Fairall, P. S. Guest, and P. O. G. Persson (2007), On the turbulent Prandtl number in the stable atmospheric boundary layer, *Boundary Layer Meteorol.*, *125*, 329–341.

Howard, L. (1961), Note on a paper of John W. Miles, *J. Fluid Mech.*, *10*, 509–512.

Huq, P., and R. E. Britter (1995), Turbulence evolution and mixing in a two-layer stably stratified fluid, *J. Fluid Mech.*, *285*, 41–67.

Itsweire, E. C., K. N. Helland, and C. W. Van Atta (1986), The evolution of grid-generated turbulence in a stably stratified fluid, *J. Fluid Mech.*, *162*, 299–338.

Jimenez, M. A., and J. Cuxart (2005), Large-eddy simulations of the stable boundary layer using the Standard Kolmogorov theory: Range of applicability, *Boundary Layer Meteorol.*, *115*, 241–261.

Kantha, L. H., and C. A. Clayson (2000), *Small Scale Processes in Geophysical Fluid Flows*, 888 pp., Academic, San Diego, Calif.

Klipp, C. L., and L. Mahrt (2004), Flux gradient relationship, self-correlation and intermittency in the stable boundary layer, *Q. J. R. Meteorol. Soc.*, *13*, 2087–2103.

Mellor, G. L., and T. Yamada (1982), Development of turbulence closure model for geophysical fluid problems, *Rev. Geophys.*, *20*, 851–875.

Miles, J. W. (1961), On the stability of heterogeneous shear flows, *J. Fluid Mech.*, *10*, 496–508.

Noh, Y., Y. J. Kang, T. Matsuura, and S. Iizuka (2005), Effect of the Prandtl number in the parameterization of vertical mixing in an OGCM of the tropical Pacific, *Geophys. Res. Lett.*, *32*, L23609, doi:10.1029/2005GL024540.

Pacanowski, R. C., and S. G. H. Philander (1981), Parameterization of vertical mixing in numerical models of the tropical oceans, *J. Phys. Oceanogr.*, *11*, 1443–1451.

Peters, H., M. C. Gregg, and J. M. Toole (1988), On the parameterization of equatorial turbulence, *J. Geophys. Res.*, *93*, 1199–1218.

Piccirillo, P., and C. W. Van Atta (1997), The evolution of a uniformly sheared thermally stratified turbulent flow, *J. Fluid Mech.*, *334*, 61–86.

Rohr, J. J., E. C. Itsweire, K. N. Helland, and C. W. Van Atta (1988), An investigation of the growth of turbulence in a uniform mean shear flow, *J. Fluid Mech.*, *187*, 1–33.

Stewart, E. J., and P. Huq (2006), Dissipation rate correction methods, *Exp. Fluids*, *40*, 405–421.

Sukoriansky, S., and B. Galperin (2005), A spectral-closure model for turbulent flows with stable stratification, in *Marine Turbulence: Theories, Observations and Models*, edited by H. Baumert, J. Simpson, and J. Sündermann, chap. 6, pp. 53–65, Cambridge Univ. Press, Cambridge, U. K.

Sukoriansky, S., B. Galperin, and I. Staroselsky (2005), A quasi-normal scale elimination model of turbulent flows with stable stratification, *Phys. Fluids*, *17*, 085107, doi:10.1063/1.2009010.

Tennekes, H., and J. L. Lumley (1982), *A First Course in Turbulence*, 300 pp., MIT Press, Cambridge, Mass.

Turner, J. S. (1973), *Buoyancy Effects in Fluids*, 368 pp., Cambridge Univ. Press, Cambridge, U. K..

Yague, C., G. Maqueda, and J. Rees (2001), Characteristics of turbulence in the lower atmosphere at Halley IV station, Antartica, *Dyn. Atmos. Oceans*, *34*, 205–223.

Zilitinkevich, S. S., T. Elperin, N. Kleeorin, and I. Rogachevskii (2007), Energy- and flux-budget (EFB) turbulence closure model for stably stratified flows, *Boundary Layer Meteorol.*, *125*, 167–191.

P. Huq, College of Marine and Earth Studies, University of Delaware, Newark, DE 19716, USA. (huq@udel.edu)

E. J. Stewart, Visual Numerics Inc., 12657 Alcosta Boulevard, Suite 450, San Ramon, CA 94583, USA.